sustainability

MDPI

Article

Research on Hole Collapse Monitoring Technology of Coal Seam Gas Extraction Boreholes

Renhui Cheng [1,2,*], Chao Zhang [1,2], Fuhuai Fan [1,2], Chenye Duan [1,2] and Zhiheng Chen [1,2]

[1] College of Safety Science and Engineering, Xi'an University of Science and Technology, Xi'an 710054, China; zc@xust.edu.cn (C.Z.)
[2] Key Laboratory of Western Mine Exploitation and Hazard Prevention of the Ministry of Education, Xi'an 710054, China
* Correspondence: crhalzj@126.com; Tel.: +86-17636145802

Abstract: It is difficult to monitor the collapse position of a gas extraction borehole in a coal seam. In order to solve this problem, a fiber-optic grating collapse monitoring technology was proposed. Five kinds of grating arrangements (0°, 45°, 90°, 135°, 180°) were examined to simulate the hole collapse. The relationship model between the center wavelength offset and the amount of collapsed coal and extraction flow was constructed to obtain the distribution curve of the hole collapse position and quality along the length of the hole, and flow decay rates of 80% and 50% were used as the critical values to classify the three levels of hole collapse. The results show that the hole collapse monitoring accuracy is the highest with the grating measurement points located below the substrate material arrangement. Finally, the effectiveness of fiber-optic grating monitoring technology was verified in the 2202 working face of the Changcun coal mine of the Lu'an Group, and the pure amount of gas extraction from the repaired borehole after monitoring was increased by 62.6% compared with that before the repair.

Keywords: gas extraction; drilling hole collapse monitoring; fiber grating; wavelength shift

Citation: Cheng, R.; Zhang, C.; Fan, F.; Duan, C.; Chen, Z. Research on Hole Collapse Monitoring Technology of Coal Seam Gas Extraction Boreholes. *Sustainability* **2023**, *15*, 10262. https://doi.org/10.3390/su151310262

Academic Editors: Yabin Gao, Ziwen Li and Tong Liu

Received: 17 May 2023
Revised: 23 June 2023
Accepted: 26 June 2023
Published: 28 June 2023

1. Introduction

China's coal seams have complex and variable endowment conditions, and mines are prone to serious gas disasters [1–4]. In the process of gas management, the hole formation quality of a gas extraction borehole is an important factor in determining the efficiency of gas extraction [5–9]. Under the influence of ground stress and mining, gas extraction boreholes are prone to collapse and deformation, which seriously affects gas management [10,11]. Borehole monitoring is a prerequisite to solving the problem of borehole collapse, can obtain the status information of the borehole, and can effectively prevent the occurrence of borehole collapse, as well as provide services to optimize the arrangement of the borehole, playing a positive role in deepening the process of drilling refinement operation, and greatly improving the effect of gas extraction in a borehole [12–15]. In order to meet the increasingly rigorous engineering research environment and achieve the goal of accurate drilling support, it is important to carry out research on accurate monitoring of the in-hole conditions of gas extraction boreholes.

With the advancement of drill-hole refinement, the traditional drill-hole collapse monitoring technology cannot achieve the goal of drill-hole refinement. Currently, the borehole flushing fluid method [16], the sonic method [17], and the endoscopic method [18] are mostly used in borehole deformation monitoring. Studies [19] have monitored borehole collapse, overburden damage, etc., by the drilling flushing fluid method. Studies [20–26] have used the acoustic method to analyze the morphology and effective radius of peripore fractures. Studies [27–29] have investigated borehole stability by observing peripore fracture development through the borehole peephole method. The drilling flushing fluid method is mainly based on the drilling effect to indirectly determine the situation in the

hole, whereas the acoustic method and the endoscopic method for the drilling hole section are better; with an increase in the hole depth, the equipment is not easy to send and video capture is not clear, so the monitoring effect is not ideal. The above methods of monitoring boreholes are not suitable for monitoring the collapse of gas extraction boreholes in a coal seam. There is an urgent need to propose an accurate monitoring technology for boreholes in order to grasp the information of boreholes dynamically and take corresponding measures to support the destabilization-prone areas of boreholes in advance to improve the gas extraction rate.

A fiber grating strain sensor is a high-precision monitoring element with an optical signal as the transmission carrier; this has the advantages of extreme anti-electromagnetic interference, corrosion resistance, water and moisture resistance, and low transmission loss and is widely used in underground engineering fields, such as rock and coal mines. Studies [30–32] have monitored borehole surrounding rock pressure by strain-grating sensors. Studies [33–39] have applied fiber-optic grating monitoring technology to mine pressure monitoring, such as sudden water in the roof and floor of coal seams. Studies [40] have applied grating sensors to the stress monitoring of anchor rods in roadways. At present, there are few studies on the application of fiber-optic grating monitoring technology for borehole collapse monitoring; however, all the above-mentioned scholars' studies have shown the feasibility of fiber-optic grating applications in underground coal mines and even in boreholes.

Based on the above analysis, this paper proposes a hole collapse monitoring technology based on fiber-optic grating for an unknown hole collapse situation, explains the principle of fiber-optic grating hole collapse monitoring, builds a physical simulation experiment platform to carry out hole simulation experiments of five grating arrangements (0°, 45°, 90°, 135°, 180°) with different collapsed coal volumes, studies the wavelength shift of the grating measurement and the variation law of the extraction flow rate with the collapsed coal volume, and classifies the hole collapse level and validates it in the field. The change law of the wavelength offset and extraction flow rate with the amount of collapsed coal was studied, and the hole collapse level was classified and verified in the field. The proposed fiber-optic grating hole collapse monitoring technology can determine the location of a hole collapse in advance so that timely measures can be taken to repair the hole and ensure efficient gas extraction. This is expected to provide a scientific basis for accurate drill-hole support and provide a basis for coal mines to obtain real-time information about the drill hole and facilitate better guidance for gas extraction from the drill hole.

2. Fiber Grating Collapse Monitoring Principle

Fiber grating is formed when light causes the fiber to produce a periodic change in the refractive index in the axial direction, forming a phase grating in permanent space [41,42]. Fiber Bragg grating hole collapse monitoring is mainly achieved through fiber Bragg grating stress sensors, which are attached to the substrate material and protected by packaging. The overall structure mainly consists of a core, cladding, and a coating layer structure. When the fiber grating is stimulated by the external environment, such as knocking the amount of collapsed coal, the grating pitch on the internal core changes, resulting in changes in the propagation path of the reflected light, causing changes in the wavelength offset of the received light signal, and this change in the received wavelength offset can characterize the physical signal given by the external stimulus affecting the grating pitch change.

In order to monitor the collapse situation in the borehole, a surface-mounted encapsulated fiber grating sensor was selected. As shown in Figure 1, when hole collapse deformation occurs, the amount of collapsed coal causes the deformation of the sensor substrate material, and the optical signal reflected from the grating measurement points at different locations from the deformation has different wavelength shifts. When the coal collapse occurs near measurement point B, the wavelength offset of the center of the light signal reflected back from measurement point B is larger, the measured wavelength offset of the adjacent measurement point C is smaller, and the wavelength offset of measurement

point A does not change because there is no coal fall. The location of the collapsed borehole can be determined by the arrangement of the measurement points and the location of the measurement point where the offset occurs in the borehole, and the quality of the collapsed coal in the borehole near the measurement point can be inferred from the change in the wavelength offset reflected from the measurement point, thus realizing the monitoring of the collapsed borehole location.

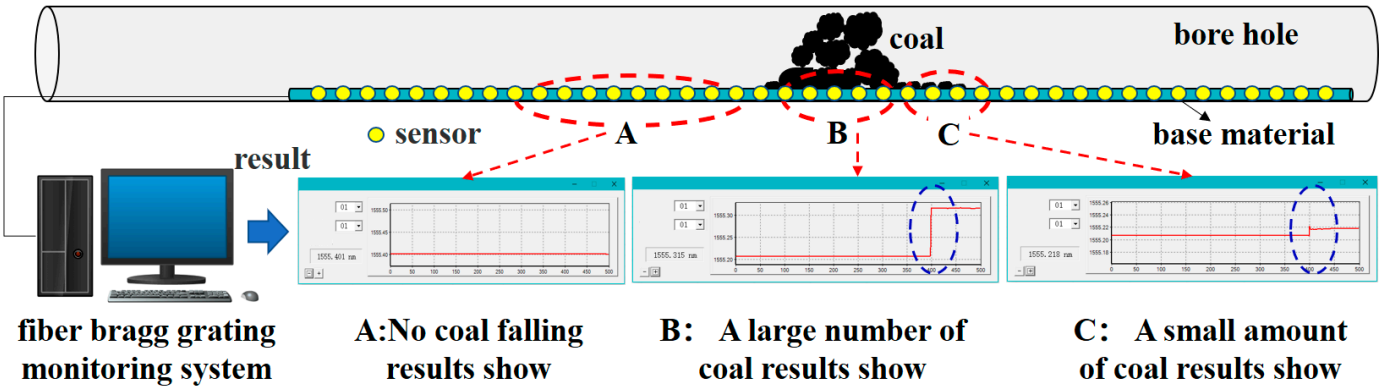

Figure 1. Fiber-optic grating sensor positioning principle.

3. Experiment

In order to achieve fiber grating monitoring of a borehole collapse, it is necessary to determine the arrangement of fiber grating sensors in the borehole to achieve the accurate monitoring of a borehole collapse. In this study, we investigated the accuracy of monitoring hole collapse at different locations in the substrate.

3.1. Experimental System Construction

According to the above fiber grating hole collapse monitoring principle, the experimental simulation platform for fiber grating hole collapse characterization was built, as shown in Figure 2. A PVC pipe with a diameter of 120 mm was used to simulate the borehole, and a tee was installed in the middle of the pipe to simulate the collapsed hole location. A demodulator and a host computer were connected to the outside of the pipe to receive fiber-optic data, while a flow meter and a vacuum pump were connected to simulate the borehole flow extraction at a maximum pumping rate of 30 L/min.

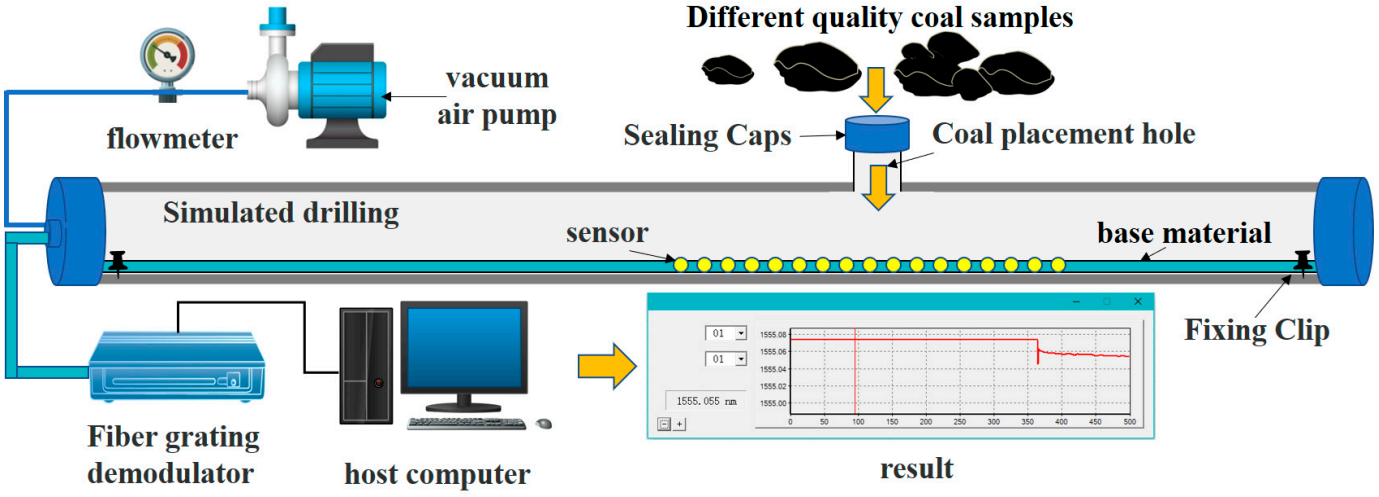

Figure 2. Schematic diagram of the experimental platform system.

In the experiments, a fiber grating measurement point grating length, L, of 10 mm and a central wavelength, λb, between 1555 and 1565 nm were used; the reflectivity, neff,

was 93.69%, and the edge film rejection ratio was 15~16 dB. In the practical application of a fiber grating sensor, the grating monitoring accuracy is greatly affected by the grating encapsulation effect, and the surface paste encapsulated grating measurement accuracy is mainly affected by the substrate material and paste layer. The measurement accuracy of the surface mount grating is mainly affected by the substrate material and the characteristics of the mount layer. The substrate material of the surface-mounted optical fiber grating was a PVC pipe, and the adhesive layer was a two-component heat-curing epoxy resin adhesive (353 ND). After curing, the length of the adhesive layer was about 20 mm, the width was about 10 mm, and the thickness of the adhesive layer was about 1 mm.

3.2. Experimental Protocol

The monitoring results of the experiments were different when the selected surface-mounted fiber grating sensor and substrate material were in different positions to monitor the stress changes. In order to investigate the effect of the sensor located in different positions of the substrate material on the monitoring results, the typical angle was selected to design five groups of experiments of fiber grating deflection, 0°, 45°, 90°, 135°, and 180°, which were recorded as Groups A, B, C, D, and E, as shown in Figure 3.

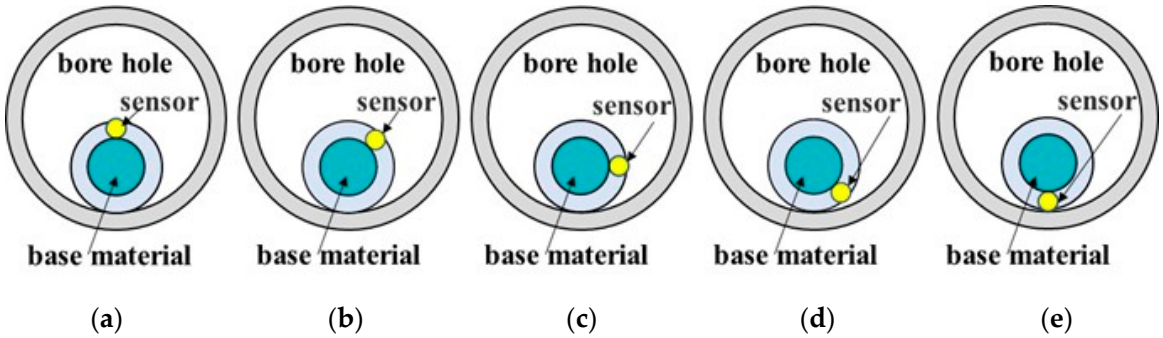

Figure 3. Surface-mounted fiber grating. (**a**) Deflection 0°, (**b**) Deflection 45°, (**c**) Deflection 90°, (**d**) Deflection 135°, and (**e**) Deflection 180°.

Based on the above fiber grating collapse monitoring principle, the experiment characterized the quality of the collapsed coal volume by the wavelength offset. The curve change of the fiber grating wavelength was monitored in real time, and the difference in the grating measurement wavelength before and after the curve change was the fiber grating measurement wavelength offset. The specific steps were as follows:

① Equipment connection. The PVC pipe with a fiber-optic grating sensor was fixed on the drilling simulation platform, the grating encapsulation area was located at the side of the direct coal fall, and the fiber was connected to the debugged fiber-optic grating demodulator through the FC interface on the plug; the two ends of the drilling simulation platform were sealed with plugs to check the overall air tightness of the experimental system.

② Coal sample preparation. Coal samples were taken from the 2202 working face of the Changcun coal mine of the Shanxi Lu'an Group. The coal samples were randomly crushed with different particle sizes, similar to the collapsed coal pieces of the borehole, in order to simulate the actual collapse of the borehole.

③ Simulate the collapse of coal blocks in the drill hole. The coal sample was dropped from the opening above the drilling simulation platform; the coal sample drop pipe was blocked with a sealing tube and sealed with a plug to avoid vortex flow at the lower edge of the drop pipe as much as possible and reduce the influence on the extraction data, and the pump was activated with a pumping rate of 30 L/min.

④ Record data. When the detected optical fiber grating returned the optical signal center wavelength stability, the grating center wavelength was recorded, while the experiment pumping flow changes were recorded.

⑤ Equipment finishing. The extraction simulation system was suspended, the coal samples were poured out from the other side, and the fine coal chips were cleaned up and prepared for the next set of experiments.

4. Results and Analysis

4.1. Analysis of Collapsed Coal Sample Mass and Wavelength Offset

The difference between the measured wavelength and the initial wavelength of each sample was the central wavelength shift, Δλ. The reflectance of the packaged fiber grating used in the Group B experiment (fiber grating deflected by 45°) was 93.74%, and the initial central wavelength was 1555.164 nm. The reflectance of the packaged fiber grating used in the Group C experiment (fiber grating deflection 90°) was 94.36%, and the initial center wavelength was 1555.198 nm. The reflectance of the packaged fiber grating used in the Group D experiment (fiber grating deflection 135°) was 94.52%, and the initial center wavelength was 1555.115 nm. During the experiment, the actual mass, m, of the five groups of coal samples was plotted against the measured wavelength shift in a scatter plot, as shown in Figure 4.

From the literature [43,44], it is known that when the fiber grating material is certain, the grating measurement center wavelength shift has a good linear relationship with the monitored strain; there is also a good linear relationship between the coal sample mass and the induced strain. In addition, it can be concluded that there is a linear correlation between the grating measurement wavelength shift and the coal sample mass, so the linear function is chosen to fit the scatter plot of each group of experimental data for analysis.

The red spheres in the figure represent the variation values of the wavelength offsets obtained from different angles of the sensor monitoring corresponding to different coal sample masses, the blue dotted lines represent the fitted curves of all the data, and the purple solid lines represent the fitted curves of the wavelength offsets monitored for coal sample masses from 0 to 100 g.

In Figure 4a, the fitted curve fit R^2 = 0.96065 for the experimental data from 0 to 500 g in Group A indicates that the central wavelength offset, Δλ, has a good linear relationship with the coal sample mass, m. The equation to characterize the sample mass, m, by the wavelength offset, Δλ, was $m = 4.349\Delta\lambda$. Meanwhile, it can be seen in Figure 4a that the value of the wavelength offset changes significantly after the coal sample mass exceeds 100 g, which is due to the direct knocking of the coal sample on the sensor, leading to obvious changes in the data, and the wavelength offset data corresponding to the coal sample mass from 0 to 100 g were fitted with the fit R^2 = 0.94753 and the equation. The slope of the two sets of equations changes significantly, indicating that the monitoring error is larger with the arrangement of the sensors in Group A.

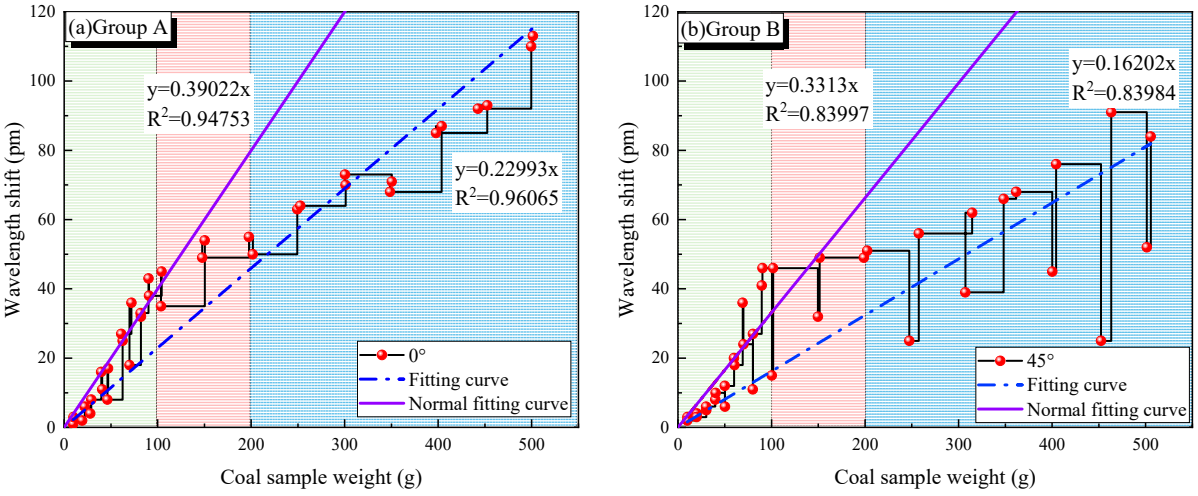

Figure 4. *Cont.*

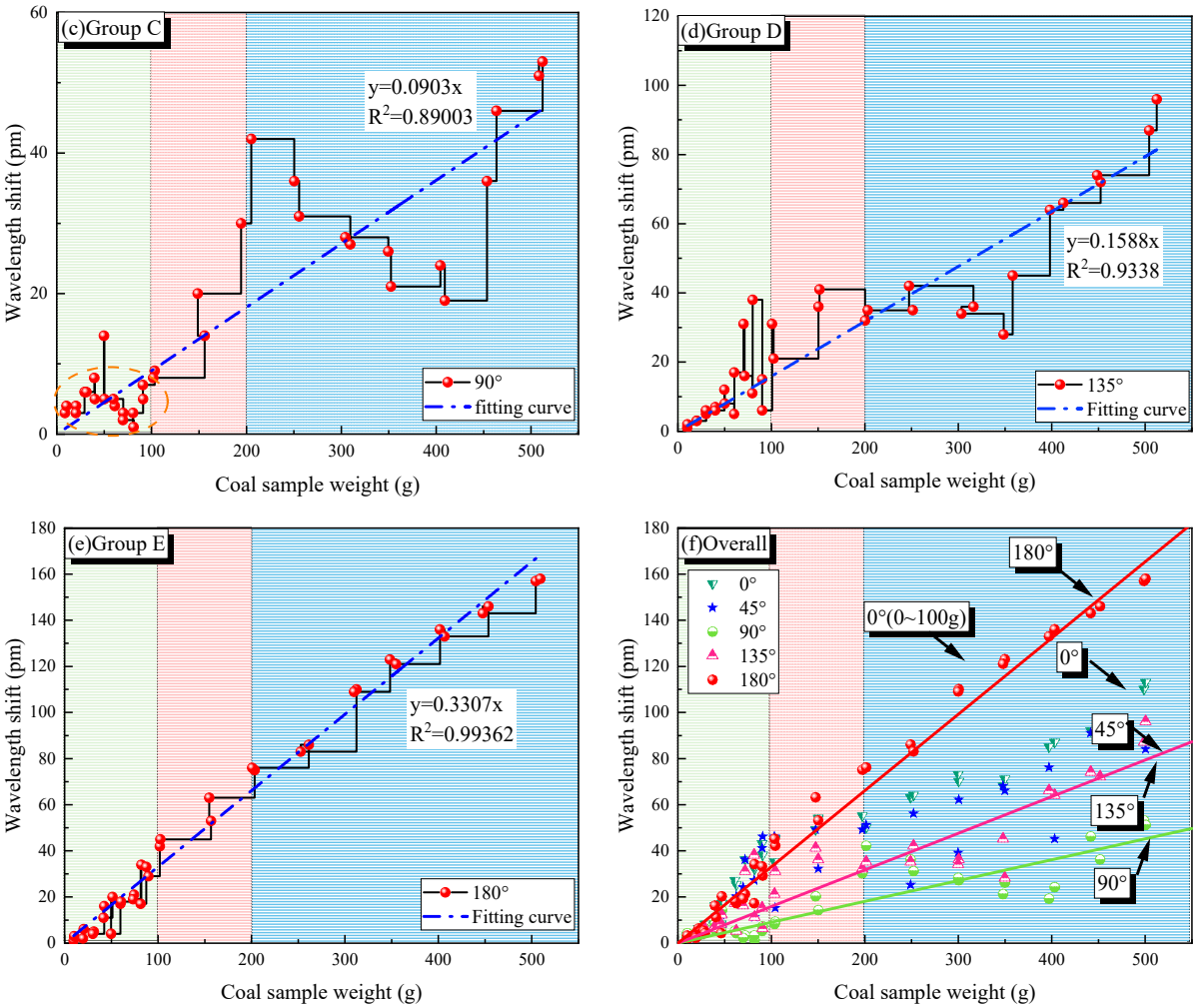

Figure 4. Fitted curves of coal sample experimental data.

Figure 4b shows the fitted curve fit R^2 = 0.83984 for the experimental data from 0 to 500 g in Group B. The equation for the wavelength shift, Δλ, characterizing the specimen mass, m, was m = 6.172Δλ. The wavelength offset corresponding to the mass of a 0~100 g coal sample was fitted with the fit R^2 = 0.83997 and the equation was m = 3.018Δλ. In Figure 4b, it can be seen that the relationship between the coal sample mass and the wavelength offset has a large deviation, with the data showing a large gap between them, and the data fit is significantly lower than that of Group A. This is due to the fact that the sensor arrangement position cannot monitor the full fallen coal mass.

In Figure 4c, the sensor arrangement is at an angle of 90° with the substrate, and the monitored data are more variable at this time. The fit of the fitted curve R^2 = 0.89003 indicates that there is a certain linear relationship between the coal sample mass, m, and the wavelength offset, at which time the wavelength offset, Δλ, characterizes the equation of the coal sample mass, m, as follows: m = 11.074Δλ.

In Figure 4d, the sensor arrangement is at an angle of 135° with the substrate, and the wavelength offset monitored at this time is more obvious after the coal sample mass is less than 100 g and the mass is more than 400 g in a linear pattern. The fit of the fitted curve is R^2 = 0.9338, and the equation of the wavelength offset, Δλ, characterizing the coal sample mass, m, is: m = 6.297Δλ. This is due to the fact that when the mass of the coal sample is less than 100 g, the knock on the sensor is smaller and the monitoring result is more sensitive; when the mass of the coal sample is more than 100 g, the volume of the coal sample becomes larger and part of the fallen coal will not act directly on the sensor, resulting in an unsatisfactory monitoring effect. When the coal sample mass is greater than

400 g, the sensor is filled around by the falling coal, and the subsequent falling coal will apply force to the sensor through the previous falling coal, so a clear linear pattern will be monitored.

In Figure 4e, the sensor is located in the lowermost part of the matrix material, the matrix material provides a protective layer for the sensor, and the falling coal acts directly on the matrix material, at which time an obvious linear law is monitored, and the fit of the fitted curve is $R^2 = 0.99362$, and the wavelength offset, $\Delta\lambda$, characterizes the equation of the coal sample mass, m, as follows: $m = 3.024\Delta\lambda$.

The masses of the coal samples selected in the experiment were 10, 20, 30, 40, 50, 60, 70, 80, 90, 100, 150, 200, 250, 300, 350, 400, 450, and 500 g. Although there were some differences in the coal samples taken in the experiment, the changes were not significant, so the five groups of experimental data were analyzed as a whole. In Figure 4f, it can be seen that the slope of the wavelength offset corresponding to 180° of sensor deflection is the largest, followed by 0°, 45°, and 135°, with 90° being the smallest, and the slope of the wavelength offset corresponding to 0° of fiber deflection is the largest when the mass of the coal sample is 0~100 g. This indicates that the knocking effect of the falling coal mass on the sensor is large, resulting in large errors in the sensor monitoring results, and when the sensor is deflected by 180°, it is protected by the substrate material, which greatly reduces the monitoring errors. At the same time, it can be seen that the matrix material serves to protect the sensor while reducing its monitoring data (i.e., slope reduction).

A comprehensive analysis of the distribution of the amount of collapsed coal during the five groups of experiments showed that the grating measurement points of Group A were arranged toward the top, and the grating measurement points are easily damaged when there is a large mass of coal collapse. The arrangement of the grating measurement points in Groups B, C, and D will have a "monitoring blind zone" on the other side because the collapsed coal blocks in the borehole tend to fill the space on both sides of the PVC pipe; at this time, the collapsed coal mass characterized by the grating measurement wavelength offset can only reflect part of the actual collapsed coal volume, which is also the main reason for the poor linearity of the monitoring data in Groups B, C, and D. The arrangement of the measurement points in Group E can effectively avoid the destruction of the grating measurement points when the coal blocks the collapse. At the same time, from the experimental data of each group, it can be seen that the linear relationship between the Group E specimen monitoring data is optimal, i.e., when the grating deflection angle is 180°, the function relationship between the central wavelength offset, $\Delta\lambda$, and the specimen mass, m, is the most obvious, so the Group E grating point arrangement was adopted for the borehole collapse monitoring technology, i.e., the grating points were arranged below the matrix material.

4.2. Analysis of the Relationship between Wavelength Offset and Extraction Flow

The actual single-hole gas extraction flow rate in the field is often affected by a variety of factors, and the experiment only considered the effect of collapsed holes on the gas extraction flow rate of the borehole. The scatter plot of the obtained extraction simulation data was fitted with the wavelength offset of the coal sample to obtain several sets of fitted relationships between the extraction flow rate and wavelength offset, as shown in Figure 5.

The flow rate can characterize the hole collapse situation: the more serious the hole collapse, the larger the wavelength offset and the smaller the flow rate. As can be seen from Figure 5, the fit between the wavelength offset and the flow rate for Groups B, C, and D is not high, which is due to the fact that the sensors are located on both sides of the matrix material and can only monitor part of the coal fall, resulting in a decrease in the borehole flow rate but a small change in the wavelength offset. The fit $R^2 = 0.95545$ of the fitted curve of Group A indicates that the monitoring result of Group A is better and can characterize the hole collapse situation of the borehole, while it can be seen that the borehole flow gradually slows down with an increase in the wavelength offset, which is due to the direct knocking of the coal body by the falling coal causing certain damage to the

wireless sensor, resulting in the slowdown of the borehole flow curve at a later stage. For the goodness-of-fit R^2 = 0.98805 for the fitted curve of Group E, it is obvious that all the data are distributed around the fitted curve, and the approximate linear trend decreases, indicating that the monitoring results are most accurate at this time. As can be seen from Figure 5e, the sensor deflection angle is 180°, that is, when it is located in the lower part of the matrix material, the wavelength offset decreases simultaneously as the flow rate decreases, and the wavelength offset of the rest of the monitoring data cannot fully reflect the hole collapse situation of the borehole. It can be clearly seen from Figure 5f that the data fitting effect of Group E is the best. Based on the above study, the accuracy of the Group E grating point arrangement of the borehole collapse monitoring technology is proved again, that is, the grating points are arranged below the matrix material, and the relationship between the wavelength offset and the flow rate is $Q = 1.490 \times 10^{-6}\Delta\lambda^3 + 1.291\Delta\lambda^2 - 0.183\Delta\lambda + 29.975$.

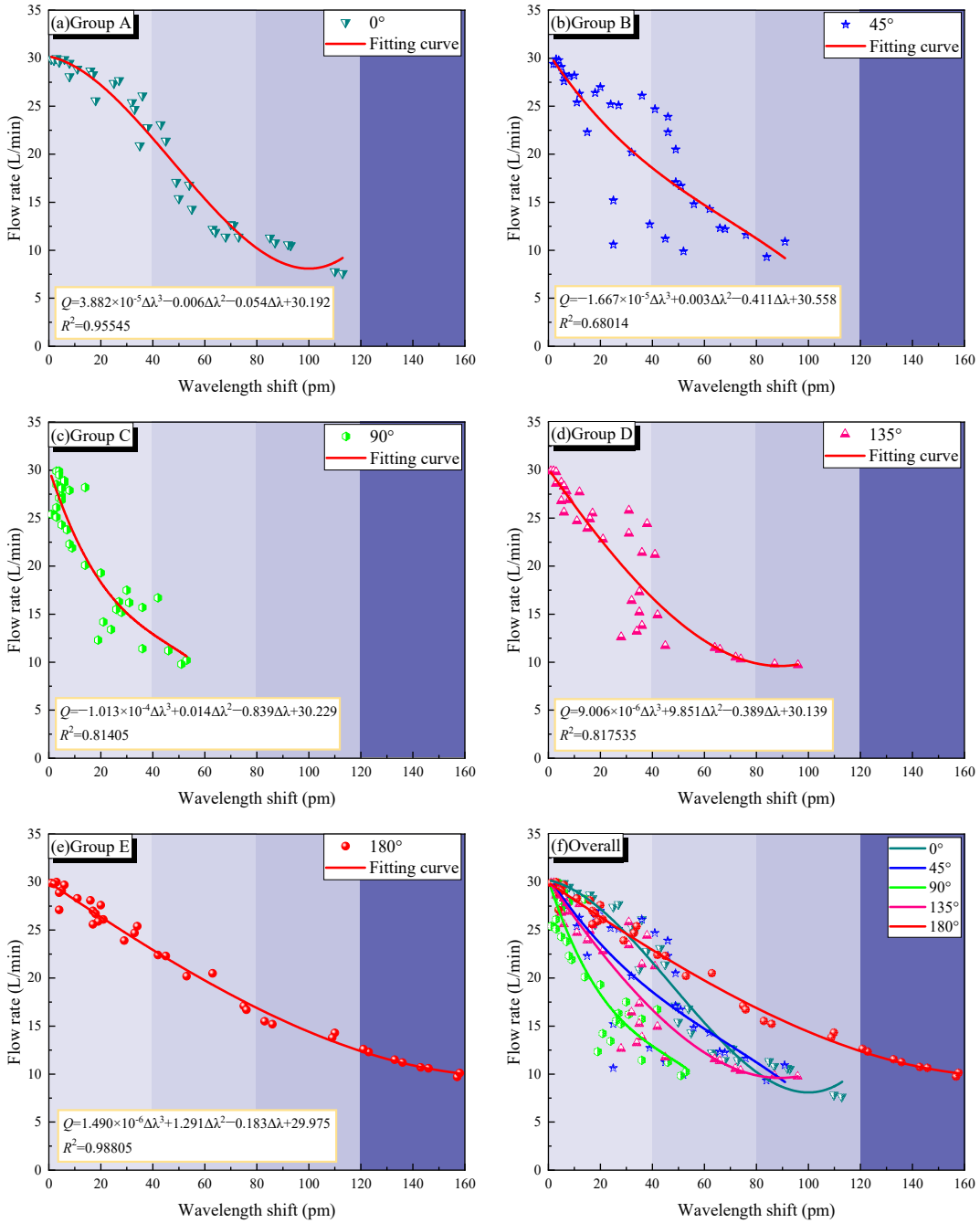

Figure 5. Fitting curves of simulated extraction experimental data.

4.3. Severity of Hole Collapse Classification

From the above experimental results, it can be seen that the relationship between the central wavelength offset, Δλ, and the sample mass, m, and the extraction flow rate, Q, is more obvious, so the amount of collapsed coal and the extraction flow rate can be characterized by monitoring the change in the wavelength offset. With the detected wavelength offset as the horizontal coordinate, the mass and flow rate data obtained from the Group F experiments were summarized and are shown in Figure 6.

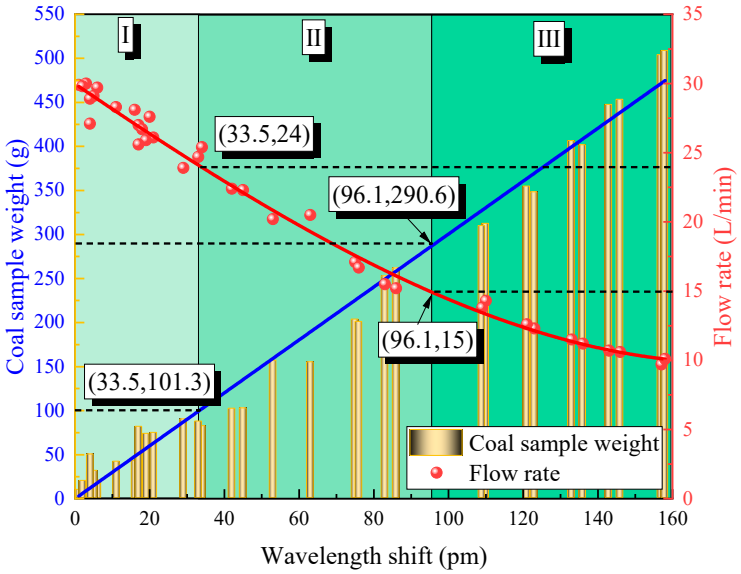

Figure 6. Experimental data and collapsed holes of Group E.

The equation of the fitted curve between the wavelength offset, Δλ, in the center of Group E and the experimental data of the specimen mass, m, is $m = 3.024\Delta\lambda$. The decay ratio of the drill-hole extraction flow is used as the evaluation index, the wavelength offset is used to characterize the amount of collapsed coal, and the actual drill-hole collapse can be classified into three grades according to the two critical indicators of the reduction of the drill-hole extraction flow to 80% and 50% (see Table 1).

Table 1. Drill-hole collapse grade classification.

Collapsed Hole Grade	Flow Rate (L/min)	Wavelength Shift (pm)	Coal Sample Weight (g)	Extraction Efficiency (%)	Hole Collapse Situation
Grade I	24~30	0~33.5	0~101.3	80~100	Slightly collapsed hole
Grade II	15~24	33.5~96.1	101.3~290.6	50~80	More serious hole collapse
Grade III	0~15	>96.1	>290.6	0~50	Severe hole collapse

5. Field Test

In order to better verify the fiber-optic grating collapse hole monitoring technology, the 2202 working face of the Changcun coal mine of Shanxi Lu'an Environmental Protection Energy Development Company Limited was selected for the field test. The Changcun coal mine belongs to a high gas mine, in which the inclined length of the 2202 working face is about 249.28 m, the strike length is 1076.86 m, the average thickness of the coal seam is 6.35 m, and the recoverable reserve is about 211.77 million tons.

The drilling arrangement is a three-flower arrangement, with 1.8 m for the high hole and 1.6 m for the low hole; the length of the hole is 120 m, the diameter of the hole is 94 mm, and the distance between the holes is 2 m.

A total of five boreholes were monitored on site, starting from 20 m after the borehole opening (skipping the sealed section of the borehole), with a monitoring length of 120 m and an average of one monitoring point set at 1 m. Among the five boreholes monitored, the collapse of Borehole No. 2 was relatively mild, with only a small area collapsed and the highest collapse grade reaching Grade II; the collapse of Boreholes No. 1, No. 3, No. 4, and No. 5 was more serious, all reaching Grade III. In this study, the monitoring data of Borehole No. 3 were used as an example for analysis, and the results of the borehole wavelength offset from the monitoring of the first day, 7 days, and 30 days after the completion of the borehole sealing are shown in Figure 7:

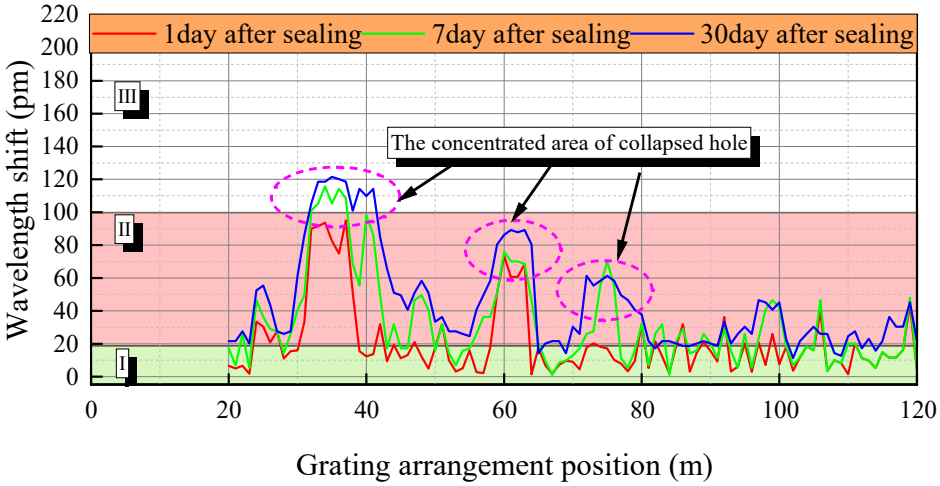

Figure 7. Variation of the wavelength offset of the borehole after 1, 7, and 30 days after sealing.

In Figure 7, the green, red, and white sections represent the collapse grade of the borehole as Grades I, II, and III, respectively. As can be seen from Figure 7, after excluding the influence of small coal pieces on the grating signal after retreating from the drill hole, there were mainly two places that reached Grade II on the first day after the completion of the sealing work, which were located at 31–38 and 59–63 m, with a mass of collapsed coal body of 1787.8 and 921.1 g, respectively. Five places reached Grade II 7 days after the completion of the drill hole, which were located at 24–26, 29–49, 57–64, 72–76, and 97–100 m. One month after the completion of the hole, the collapse situation was stable, and there were four collapsed holes of Grade II, which were located at the measurement points of 24~64, 70~81, 97~100, and 116~119 m. In addition, a serious collapse occurred at 30–43 m near the hole entrance within one month after the hole was completed.

Overall, Figure 7 shows that after a hole collapse occurs in the borehole after sealing is completed, the situation of the hole collapse near this section will gradually increase with gas extraction, and the collapse area will be appropriately enlarged; therefore, it can be seen that the collapse data monitored on the first day can provide a reference for the collapse area of the borehole later. Therefore, in the actual mine engineering operation, monitoring of the borehole can be carried out at the completion of the drilling operation to determine the hole collapse area in advance, and supporting measures can be made to reduce the occurrence of the hole collapse.

By processing the collapsed holes obtained from the monitoring by the drilling support, such as placing screen tubes and hydraulic punching, the extraction data from 30 days before and after each of the four holes were counted, as shown in Figure 8. The lowering of the sieve pipe meant that a PVC pipe with an eyelet was placed into the borehole through the drill stem piece to monitor the collapsed area. Hydraulic punching is mainly for boreholes with light collapse, where the collapsed area is directly flushed with the help of high-pressure water.

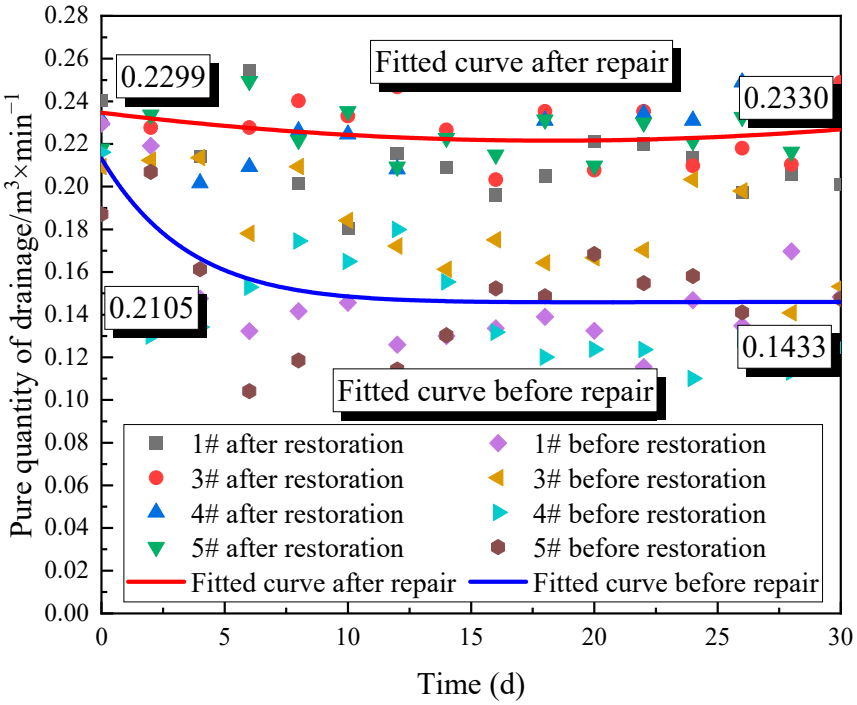

Figure 8. Comparison of extraction data before and after hole rehabilitation.

In Figure 8, the red line is the fitted curve of the extraction data after the drilling support, and the blue line is the fitted curve of the extraction data before the support. In this figure, only the pure extraction data before and after the support of Boreholes No. 1, No. 3, No. 4, and No. 5 are compared and analyzed, and it can be seen that there is a significant improvement in all of them. The average 30 day extraction volume of the borehole after the support was 0.2330 m^3/min, which is 62.6% higher than 0.1433 m^3/min before the support.

6. Conclusions

(1) Fiber-optic grating collapse monitoring technology for gas boreholes in this coal seam was proposed, and the principle of fiber-optic grating collapse monitoring was explained. Based on the principle of the grating distance change caused by the deformation of the substrate material of a surface-mounted fiber-optic grating sensor, the amount of coal collapse in the borehole was characterized by the grating measurement wavelength offset, and the amount of coal collapse in the borehole was monitored by arranging the grating measurement points in the borehole to monitor the collapse of the borehole.

(2) A physical simulation test of the collapsed gas extraction borehole was carried out, five grating arrangements of 0°, 45°, 90°, 135°, and 180° deflection were designed, and the arrangement with the grating measurement point located below the substrate material (i.e., Group E) was obtained, with the highest accuracy of collapsed borehole monitoring and the optimized arrangement of the grating sensor measurement point location.

(3) The calculation model of the central wavelength offset, Δλ, and the collapsed coal volume, m, was constructed as $m = 3.024\Delta\lambda$. The drilling hole collapse degree classification was realized, and the drilling hole collapse degree was classified into three levels according to the original extraction flow thresholds of 80% and 50%.

(4) An on-site monitoring test was carried out in the 2202 working face of the Changcun coal mine of the Lu'an Group. The distribution curve of the hole collapse position and the quality along the length of the hole was successfully obtained, and the pure extraction volume of the test hole after support was increased by 62.6% compared with an unsupported one, which verified the effectiveness of the monitoring technology.

Author Contributions: R.C.: Conceptualization, Methodology, Writing—original draft. C.Z.: Investigation, Project administration. F.F.: Supervision, Investigation. C.D.: Writing—review and editing. Z.C.: Validation. All authors have read and agreed to the published version of the manuscript.

Funding: This research was funded by the National Natural Science Foundation of China (Grant Nos. 51974241; 52174203).

Institutional Review Board Statement: Not applicable.

Informed Consent Statement: Not applicable.

Data Availability Statement: Not applicable.

Conflicts of Interest: The authors declare that they have no known competing financial interests or personal relationships that could have appeared to influence the work reported in this paper.

References

1. Du, X.H.; Xue, J.H.; Ma, Q.; Chen, Z.H.; Zhan, K.L. Energy Evolution Characteristics of Coal-Rock Composite Bodies Based on Unidirectional Load. *Nat. Resour. Res.* **2022**, *31*, 1647–1663. [CrossRef]
2. Du, X.H.; Xue, J.H.; Shi, Y.; Cao, C.R.; Shu, C.M.; Li, K.H.; Ma, Q.; Zhan, K.L.; Chen, Z.H.; Wang, S.L. Triaxial mechanical behaviour and energy conversion characteristics of deep coal bodies under confining pressure. *Energy* **2023**, *266*, 126443. [CrossRef]
3. Wei, S.; Ma, Z.; Li, B.; Chai, J. Study on the monitoring method of three-dimensional stress with FBG in surrounding rock and the simulation experiment. *J. Min. Saf. Eng.* **2015**, *32*, 138–143.
4. Zhang, T.; Bao, R.; Li, S.; Zhang, C.; Zhang, L. Expansion properties and creep tests for a new type of solidified expansive sealing material for gas drainage boreholes in underground mines. *Environ. Earth Sci.* **2018**, *77*, 468. [CrossRef]
5. Zhang, C.; Zeng, X.; Jiang, B.; Zhai, C.; Zhu, C.; Ni, G. Experimental study on mechanical behaviour and pore evolution of borehole-sealing materials under different confining pressures. *Arab. J. Geosci.* **2022**, *15*, 310.
6. Li, H.; Shi, S.; Lu, J.; Ye, Q.; Lu, Y.; Zhu, X. Pore structure and multifractal analysis of coal subjected to microwave heating. *Powder Technol.* **2019**, *346*, 97–108. [CrossRef]
7. Wang, Z.; Sun, Y.; Wang, Y.; Zhang, J.; Sun, Z. A coupled model of air leakage in gas drainage and an active support sealing method for improving drainage performance. *Fuel* **2019**, *237*, 1217–1227. [CrossRef]
8. Zhang, C.; Cheng, R.H.; Liu, C.; Xue, J.H.; Wang, X.L. Experimental Study on Strengthening and Sealing Materials and Their Application in Coal Mines. *Adv. Mater. Sci. Eng.* **2020**, *2020*, 6025452. [CrossRef]
9. Zhang, C.; Liu, H.; Li, S.; Liu, C.; Qin, L.; Chang, J.; Cheng, R. Experimental Study on the Expansion of a New Cement-Based Borehole Sealing Material Using Different Additives and Varied Water–Cement Ratios. *Arab. J. Sci. Eng.* **2019**, *44*, 8717–8725. [CrossRef]
10. Zhang, T.; Ling, Z.; Pang, M.; Meng, Y. Experimental Study of Creep Acoustic Emission Characteristics of Coal Bodies around Boreholes under Different Moisture Contents. *Energies* **2021**, *14*, 3103. [CrossRef]
11. Zou, X.; Qi, X.; He, L.; Hao, W. Research and Application of Plugging Technology for Abandoned Wells in High-Risk Areas. *Technol. Superv. Pet. Ind.* **2018**, *34*, 11.
12. Lines, A. Proactive interburden fracturing using UIS drilling with validation monitoring. *Int. J. Min. Sci. Technol.* **2021**, *31*, 3–7. [CrossRef]
13. Liu, J.; Liu, Z.; Wei, Y.; Chen, X. Change Characteristics of Negative Drainage Pressure along the Drill Hole: Theoretical Analyses and Field Tests. *ACS Omega* **2022**, *23*, 19948–19956. [CrossRef]
14. Lv, H.; Wang, D.; Cheng, Z.; Zhang, Y.; Zhou, T. Study on Mechanical Characteristics and Failure Modes of Coal–Mudstone Combined Body with Prefabricated Crack. *Mathematics* **2022**, *10*, 177. [CrossRef]
15. Wang, X.F.; Zhang, M.S.; Yue, Z.Q. In-situ digital profiling of soil to rock strength from drilling process monitoring of 200 m deep drillhole in loess ground. *Int. J. Rock Mech. Min.* **2021**, *142*, 104739. [CrossRef]
16. Cai, X.; Guo, Q.; Jiang, H. Utilizing Managed Pressure Drilling Technique to Prevent Rock Failure and Maintain Wellbore Stability. *IOP Conf. Ser. Earth Environ. Sci.* **2021**, *861*, 62055–62058. [CrossRef]
17. Barbosa, N.D.; Greenwood, A.; Caspari, E.; Dutler, N.; Holliger, K. Estimates of Individual Fracture Compliances Along Boreholes From Full—Aveform Sonic Log Data. *J. Geophys. Res. Solid Earth* **2021**, *126*, e2021JB022015. [CrossRef]
18. Zhao, E.; Li, K.; Yang, X.; Deng, N. Speculum Observation and Trajectory Measurement in Gas Extraction Drilling: A Case Study of Changling Coal Mine. *Geofluids* **2021**, *2021*, 5545067. [CrossRef]
19. Shi, J.; Hou, C.; Wang, S.; Xiong, X.; Wu, S.; Liu, C. The semi-analytical productivity equations for vertically fractured coalbed methane wells considering pressure propagation process, variable mass flow, and fracture conductivity decrease. *J. Pet. Sci. Eng.* **2019**, *178*, 528–543. [CrossRef]
20. Feng, X.T.; Young, R.P.; Reyes-Montes, J.M.; Aydan, Ö.; Ishida, T.; Liu, J.P.; Liu, H.J. ISRM Suggested Method for In Situ Acoustic Emission Monitoring of the Fracturing Process in Rock Masses. *Rock Mech. Rock Eng.* **2019**, *52*, 1395–1414. [CrossRef]
21. Liu, H.; Xu, F.; Dong, L.; Xiong, Y. Calculation of Filling Ratio of Fissures for Curtain Grouting by Acoustic Velocity of Rock Masses. *IOP Conf. Ser. Earth Environ. Sci.* **2021**, *660*, 12077–12079. [CrossRef]

22. Manuello, G.C.A. AE monitoring of a concrete arch road tunnel: Damage evolution and localization. *Eng. Fract. Mech.* **2019**, *210*, 279–287. [CrossRef]
23. Tailakov, O.V.; Zastrelov, D.N.; Makeev, M.P.; Saltymakov, E.A.; Kolesnichenko, S.E. Monitoring of physical condition changes in strata boreholes during coal mining. *IOP Conf. Ser. Earth Environ. Sci.* **2021**, *823*, 12004. [CrossRef]
24. Wang, Y.Q.; Peng, K.; Shang, X.Y.; Li, L.P.; Liu, Z.P.; Wu, Y.; Long, K. Experimental and numerical simulation study of crack coalescence modes and microcrack propagation law of fissured sandstone under uniaxial compression. *Theor. Appl. Fract. Mech.* **2021**, *115*, 103060. [CrossRef]
25. Chen, Z.Y.; Hao, H.J.; Hao, C.S.; Zhao, J.B.; Tian, Q.L. Study on combined extraction technology of underground long borehole and CBM ground-well fracturing. *Coal Ence Technol.* **2019**, *47*, 8.
26. Zhou, X.P.; Peng, S.L.; Zhang, J.Z.; Berto, F. Failure characteristics of coarse and fine sandstone containing two parallel fissures subjected to true triaxial stresses. *Theor. Appl. Fract. Mech.* **2021**, *112*, 102932. [CrossRef]
27. Yu, D.; Yi, X.; Liang, Z.; Lou, J.; Zhu, W. Research on Strong Ground Pressure of Multiple-Seam Caused by Remnant Room Pillars Undermining in Shallow Seams. *Energies* **2021**, *14*, 5221. [CrossRef]
28. Zhao, H.; Zhang, M.; Zhang, H.; Wang, H.; Fulai, L.I. Development and application of stability dynamic monitoring and measuring device to gas drainage borehole. *Coal Sci. Technol.* **2018**, *46*, 1.
29. Zhao, J.S.; Jiang, Q.; Lu, J.F.; Chen, B.R.; Pei, S.F.; Wang, Z.L. Rock fracturing observation based on microseismic monitoring and borehole imaging: In situ investigation in a large underground cavern under high geostress. *Tunn. Undergr. Space Technol.* **2022**, *126*, 104549. [CrossRef]
30. Juraszek, J.; Gwód-Lasoń, M.; Logoń, D. FBG Strain Monitoring of a Road Structure Reinforced with a Geosynthetic Mattress in Cases of Subsoil Deformation in Mining Activity Areas. *Materials* **2021**, *14*, 1709. [CrossRef]
31. Li, X.; Zhang, J.; Li, C.; Chen, W.; Li, R. Characteristic Law of Borehole Deformation Induced by the Temperature Change in the Surrounding Rock of Deep Coalbed Methane Well. *J. Energy Resour. Technol. Trans. ASME* **2021**, *144*, 63003. [CrossRef]
32. Li, Y.; Wang, H.; Weibing, C.; Li, S.; Zhang, Q. Stability monitoring of surrounding rock mass on a forked tunnel using both strain gauges and FBG sensors. *Measurement* **2020**, *153*, 107449. [CrossRef]
33. Chou, P.Y. The evaluation of deep groundwater recharge in fractured aquifer using distributed fiber-Bragg-grating (FBG) temperature sensors. *J. Hydrol.* **2021**, *601*, 126645. [CrossRef]
34. Guglielmi, Y.; Cook, P.; Soom, F.; Schoenball, M.; Dobson, P.; Kneafsey, T. In Situ Continuous Monitoring of Borehole Displacements Induced by Stimulated Hydrofracture Growth. *Geophys. Res. Lett.* **2021**, *48*, e2020GL090782. [CrossRef]
35. Lin, C. Design of Fiber-Optic F-P Pressure Sensor in Boreholes of Coal Mines. In Proceedings of the International Conference on Intelligent Control, Measurement and Signal Processing and Intelligent Oil Field, Xi'an, China, 23–25 July 2021.
36. Mekhtiev, A.D.; Yurchenko, A.V.; Ozhigin, S.G.; Neshina, E.G.; Al'Kina, A.D. Quasi-Distributed Fiber-Optic Monitoring System for Overlying Rock Mass Pressure on Roofs of Underground Excavations. *J. Min. Sci.* **2021**, *57*, 354–360. [CrossRef]
37. Ren, Z. Research on new FBG soil pressure sensor and its application in engineering. *Opt. Z. Fur Licht-Und Elektron. J. Light-Electronoptic* **2019**, *185*, 759–771. [CrossRef]
38. Wang, X.; Xu, Z.; Sun, Y.; Zheng, J.; Zhang, C.; Duan, Z. Construction of multi-factor identification model for real-time monitoring and early warning of mine water inrush. *Int. J. Min. Sci. Technol.* **2021**, *31*, 853–866. [CrossRef]
39. Yu, G.; Yuan, L.; Ren, B.; Li, L.; Mu, W. Big data cloud platform for monitoring and early warning of water disaster from coal floor and its application feasibility in Huaihe Energy Group. *Meitan Xuebao/J. China Coal Soc.* **2021**. [CrossRef]
40. Hu, T.; Bu, S.; Hu, Z.; Wang, Y. Experimental Study on the Displacement Sensor of Coal Roadways Roof Settlement Based on Distributed Fiber Optic Sensing. *IEEE Sens. J.* **2021**, *21*, 13870–13876. [CrossRef]
41. Jiang, K.; Liang, L.; Dai, S.; Wang, H.; Song, Z.; Li, C. High-frequency fiber Bragg gating accelerometer and strain sensor-based blast test on a concrete slab. *Appl. Opt.* **2022**, *61*, 554–562. [CrossRef]
42. Lü, R.D.; Chen, T.; Pham, X.T.; Si, J.H.; Hou, X. Application of Fiber Lasers Based on Femtosecond Laser Inscribed Fiber Bragg Gratings. *Laser Optoelectron. Prog.* **2020**, *57*, 111426.
43. Guo, Y.X.; Xiong, L.; Kong, J.Y.; Zhang, Z.Y.; Qin, L. Sliding type fiber Bragg grating displacement sensor. *Opt. Precis. Eng.* **2017**, *25*, 50–58.
44. Zhang, Y.; Tian, Y.; Fu, X.; Bi, W.; Wang, H. Adjustable range draw-wire type fiber Bragg grating displacement sensor. *Guangdian Gongcheng/Opto-Electron. Eng.* **2017**, *44*, 626–632.